Materials Science & Engineering A 698 (2017) 1–11

Contents lists available at ScienceDirect

Materials Science & Engineering A

journal homepage: www.elsevier.com/locate/msea

Strain path dependence of anisotropic microstructure evolution on low Stacking Fault Energy F138 steel

N.S. De Vincentis[a,*], M.C. Avalos[a], A. Kliauga[b], H-G. Brokmeier[c,d], R.E. Bolmaro[a]

[a] Instituto de Física Rosario, FCEIA-UNR-CONICET, Bv. 27 de Febrero 210 bis, S2000EZP Rosario, Argentina
[b] Departamento de Engenharia de Materiais - Universidade Federal de São Carlos, Rodovia Washington Luís, km 235 - SP-310, São Carlos, SP 13565-905, Brazil
[c] Institut für Werkstoffkunde und Werkstofftechnik, TU Clausthal, Agricolastr. 6, 38678, Germany
[d] Helmholtz-Zentrum Geesthacht, GEMS Outstation, Notkestr. 85, 22607 Hamburg, Germany

ARTICLE INFO

Keywords:
Microstructure anisotropy
X-ray diffraction
Electron Backscatter Diffraction

ABSTRACT

Severe Plastic Deformation (SPD) techniques are widely used nowadays because of the mechanical properties improvements caused by grain refinement and development of dislocation arrays. Diffraction techniques can be used to assess the changes registered in the microstructure through these methods. Two sets of samples of F138 austenitic stainless steel were analyzed in this paper: one set was deformed by ECAE up to two pressings at room temperature, and the other set was cold rolled to 70% reduction and annealed at 600, 700, 800 and 900 °C for 1 h. The microstructural changes were determined using X-Ray diffraction and EBSD, combining both, global and local information and characterizing domain sizes, dislocation and stacking fault densities and misorientation degree and distribution caused by the different thermomechanical processing. It was observed that, despite cold rolling and 2 ECAE passes rendered rather similar von Mises deformations, the microstructure through each deformation method was different: 2 ECAE passes seem to be more effective for grain refinement and generation of equiaxed domains than cold rolling. The more significant twin activation observed in the former sample, because of continuous strain path change, may explain the difference, although dislocation densities and mechanical properties did not differ substantially for both deformation methods.

1. Introduction

One of the most known effects of deformation is the reduction of grain size, although the very concept of grain size admits a few interpretations. Together with grain refinement the accumulation of dislocations, and the many different structures in which they can be arranged, are also responsible for the complex microstructures and consequently developed mechanical properties. In fact, both effects are intimately related and it is not possible to analyze them independently. Not less worthy to be mentioned is the phenomenon of twining; for FCC metals and alloys the Stacking Fault Energy (SFE) determines the main mechanisms acting during plastic deformation. In high to medium SFE alloys, e.g. Al, Ni and pure Cu, the microstructure evolves through the formation of dislocation cells [1]. In low Stacking Fault Energy (SFE) alloys, such as austenitic stainless steels, brass and Cu-Al alloys, the metals develop deformation twins and second-generation microbands rather than dislocation cells [2]. The extent to which deformation by dislocation glide or twinning are active is directly related to the strain rate, deformation mode and temperature as well as initial grain size [3].

A technique for microstructure evaluation and characterization, that has achieved a high degree of accuracy during the last past decades, is X-ray peak broadening analysis, which allows the estimation of grain sizes and dislocation densities [4]. The technique has been recently improved by the introduction of modified Williamson-Hall and Warren-Averbach analysis by Ungár et al. [5,6]. Despite the Williamson-Hall technique is not meant to be quantitatively accurate it provides semi-quantitative data that, if used in a context and for a single material, can be of great value for characterizing the microstructure. The technique has been further refined and extended to characterize other defects like twins and stacking faults [7]. Whole Pattern Fitting (WPF) techniques relay on the simultaneous fit of several peaks. Among the existent few implementations the Convolutional Multiple Whole Pattern fitting (CMWP) is available for the calculation of the different parameters and physical variables [8].

The quantitative accuracy of X-ray diffraction technique has a drawback, which is the absence of local information. Electron Backscatter Diffraction (EBSD), on the other hand, provides point-to-point misorientation or deformation distribution in the surface of a sample. Implemented in an SEM, and with the aid of orientation imaging analysis software, it is possible to index the Kikuchi patterns

* Corresponding author.
E-mail address: devincentis@ifir-conicet.gov.ar (N.S. De Vincentis).

http://dx.doi.org/10.1016/j.msea.2017.05.033
Received 30 March 2017; Received in revised form 8 May 2017; Accepted 9 May 2017
Available online 10 May 2017

and to obtain quantitative data regarding pixel orientation, misorientation borders, inverse pole figure maps, etc. This technique is extremely useful for studying deformation on a material, detecting dislocations arrays that appear during this process and determining the different orientations of each subgrain structure [9].

Extra low carbon stainless steels, like 316-LVM or 316-LS (F138), present a complete absence of ferrite at low temperature and remain austenitic when subject to high deformations. They present a very low SFE (32 mJ/m^2 at room temperature) and consequently a high level of twinning during deformation [10,11]. Microstructure evolution results from the interplay between twining and dislocation arrays producing grain refinement and a hardening of complex nature. Scheriau et al. deformed 316L stainless steel by High Pressure Torsion (HPT) at variable plastic strains. At low plastic strain two deformation modes -mechanical twinning and submicron-scaled shear banding- mainly characterize the microstructure [12]. Later on, the incipient twinning leads to profuse mechanical twins with some tens of nanometers in thickness, with almost every grain transformed into a twin-matrix lamellar structure. Meanwhile the original shear banding divides the material into a debris-like structure leading to micron-sized blocks of twin-matrix lamellae. Because of the severe strains the initial coarse structural elements were transformed into a very homogeneous nanocrystalline microstructure.

The first stage of plastic deformation in the modified 316L austenitic steel is characterized as dislocation glide and dislocation multiplication [13]. When certain shear stress is reached the deformation process does not only involve dislocation glide but also micro-shear banding and mechanical twinning. The deformation twins are typically aligned parallel to the maximum local shear stress, and with progressive strain, the activation of more than one twin system within each grain results in pronounced intersections of twins. The crossing twin variants, which include an angle of approximately 65°, have formed rhombic blocks, and high dislocation densities are observed along the block-walls that hinder a further propagation of plastic deformation via dislocation glide. Extensively intersected twins construct a network pattern in the severely deformed grains, constraining the generation and mobility of dislocations. The subsequent plastic deformation is performed by the formation of nanometer and/or submicron sized shear bands.

The purpose of the current investigation is to perform a crossed examination of experimental data obtained mainly by EBSD and X-ray peak broadening analysis, on a set of F138 stainless steel samples subject to different thermo-mechanical processes. The presence of a high degree of twinning together with dislocation arrays generated by deformation creates a very complex microstructure and medium strength textures, where the common methods for evaluation of defects are not straight forwardly applicable. In a recent paper we have presented a collection of experiments and analysis with the purpose of analyzing the presence of microstructure anisotropy for the current material at increasing levels of deformation, although they were limited to temperature dependence, with experiments conducted at room temperature and at 300 °C [13]. The same material was studied in another paper, but focusing in the microstructural anisotropy developed after cold rolling and subsequent annealing [14]. The current paper is devoted to search for changing features with respect to strain path, ECAE or common rolling, at room temperature, where the accumulation of defects reach the highest level. The comparison can provide new data to hint on anisotropy and strain path influence on microstructure development.

2. Characterization techniques by means of diffraction

2.1. X-ray diffraction

Amongst the many techniques available for the analysis of the microstructure of materials, X-ray diffraction has proven to be a very useful option to determine, both quantitatively and qualitatively, the presence of linear, planar and volume defects in a material. These methods are based in the different influence of defects in the characteristics of the diffraction patterns: peak shifts are observed when residual stresses are present, peak intensity varies with crystallographic texture and peak broadening is observed in materials suffering deformation because of domain diminution and defect accumulation. Different methods have been developed since the early works by Scherrer [15], fitting the whole diffraction pattern or each peak separately in order to analyze peak broadening. One of the most used models was proposed by Williamson and Hall in 1958 (Williamson-Hall method), which consists in analyzing separately the contributions of average diffraction domain size and strain to peak broadening, being each diffraction order independent and dependent, respectively [4]. This method has been modified in order to relate the strain contribution to the presence of dislocations and to incorporate the broadening caused by stacking faults [6,7]. The model is ruled then by the following equation:

$$Breadth\cdot\mathrm{Cos}(\theta)/\lambda - \beta\ \ W_{hkl} = \ 1/d\ +\ (\pi M^{*2}\mathrm{b}^2/2)\rho^{1/2}\mathrm{C}_{\mathrm{Av,hkl}}(2\mathrm{Sin}(\theta)/\lambda)^2 \quad (1)$$

where λ is the wavelength, θ the Bragg angle, *Breadth* is the peak integral breadth corrected for the instrumental broadening (Caglioti's equation [16]), β is the stacking fault density, W_{hkl} are the Warren constants, d is the domain size, **b** is the Burgers vector, ρ is the dislocation density, M the dislocation arrangement parameter and C_{Av}^{hkl} are the average contrast factors for dislocations, related to the dislocation character (edge or screw) and to the relative orientation between the diffraction vector and the Burgers and line vectors of the dislocations. The values of these factors can be found for pure edge or screw dislocations in cubic [17] and hexagonal [18] materials. The dislocations that contribute to peak broadening are both *Statistically Stored Dislocations* (*SSDs*), which are stored in cell interior, and *Geometrically Necessary Dislocations* (*GNDs*), which can constitute misorientation boundaries [19], and the proportion of each type of dislocations is assessed by the M* parameter: lower values indicate a higher compactness of arrays (GNDs), and a larger value implies looser arrays (SSDs and Taylor type dislocations).

Certain assumptions must be made in order to use line breadth methods, such as the additivity of size, strain and stacking fault contributions to line breadth, or the Voigt or pseudoVoigt character of size and strain diffraction profiles. Convolutional Multiple Whole Profile method, on the other hand, does not need to make any of these assumptions because it performs a whole pattern fitting through Fourier analysis. On this model, implemented by Ungár and Ribárik [8], theoretical profile functions for domain size, strain, stacking faults and/or twins and instrumental broadening are calculated (according to initial values defined by the user) and convoluted, and then combined with a BackGround fitting function [20,21]. This modeled pattern is then fitted to the experimental diffraction pattern using a Levenberg-Marquardt least-squares algorithm.

2.2. Electron Backscatter Diffraction

The high resolution achieved by electron microscopy techniques has permitted the observation of very fine microstructural features, as well as distinguishing dislocations in arrays or nano-twins, but allowing only a local characterization. For this reason, the EBSD technique has been considered as a very potent technique for both, performing an orientation-misorientation analysis that assesses the strain localization and extending the local analysis to a more global scale, which might be somehow comparable and complementary to XRD microstructural analysis. This technique consists in the identification and indexation of Kikuchi patterns point by point in an area scan, obtaining in this way the local crystalline orientation. Using an analysis software, this information can be translated into local orientation and misorientation

data, along with the determination and quantification of grain characteristics and strain localization characterization. When implemented in an SEM, this technique can achieve a spatial resolution of 20–30 nm and a misorientation resolution of 0.5–1°.

One of the most interesting characteristics of this method, that confers it a great versatility regarding the quantification of features, is the requirement of the specification of a criterion that must be followed by contiguous pixels to be considered as constituents of a grain. This tool provides great flexibility in the determination of the feature to study, allowing to characterize grains and subgrains independently, for example. Once that a criteria is defined for a particular material, Grain Size (GS), Average Misorientation (GAM) and Orientation Spread (GOS) can be obtained, and boundary character can be assessed (GBCD). A local strain analysis can be performed through Kernel Average Misorientation determination (KAM), and GNDs can also be estimated in the most recent versions of EDAX-OIM. Stacking faults and other CSL boundaries can be also identified.

3. Experimental procedure

The material studied in this paper is an F138 austenitic stainless steel (composition presented in Table 1). The low nickel content in this material makes it suitable for body implants [22,23] and nuclear power applications [24,25].

The F138 steel was supplied as extruded rods that were annealed (at 1100 °C) and water quenched. This was considered as the 0X or As Received (AR) material, with an average grain size of 50 μm. Two sets of samples were created from this material: one set was deformed by ECAE once (E1X) and twice (E2X) and the other set was cold rolled to a 70% reduction (R70) and then annealed for 1 h at 600 (R70A6), 700 (R70A7), 800 (R70A8) and 900 °C (R70A9). This gives the opportunity to study the differences in the microstructural changes imparted by each deformation method (domain size, dislocation and stacking fault density, local misorientation development), and to explore in depth the capabilities of the diffraction techniques employed.

ECAE was performed at room temperature in an H-13 steel die ($\varphi = 120^\circ$ and $\psi = 20^\circ$) with 10 mm diameter cross section channels. A 90° rotation was imposed between the first and the second pass, according to B_C deformation route. In ECAE the sample deforms in shear within a small area at the intersection between two equal-diameter channels, causing no substantial change in outer dimensions; this allows to repeat the pressing many times following different routes and increase the accumulated strain, which can be estimated by:

$$\varepsilon_{ECAE} = (N/\sqrt{3})2(\cot(\Phi/2 + \Psi/2) + \Psi\mathrm{cosec}(\Phi/2 + \Psi/2)) \quad (2)$$

where φ and ψ are the corner and the die angles, respectively, and N is the number of passes [26]. For the configuration used in this paper the strain per pass is approximately 0.67.

Samples were cut from the ECAE and cold rolled and annealed samples, as presented in Fig. 1. X-ray measurements were performed at DESY, Petra III Max von Laue synchrotron source. Experiments were performed at P07 beamline using transmission geometry, with ~ 0.01427 nm wavelength and less than 0.01° angular divergence and the samples prepared as 20 mm long and 1.5 mm thick rods in order to obtain the minimum thickness contribution to peak broadening. The samples were placed on a translation-rotation stage that allowed to collect 37 Debye-Scherrer images in a 180° span around the vertical axis with 5° step rotations and a Mar345 solid state area detector with

Table 1
Composition and properties for F-138 and AISI316L, austenitic stainless steels.

Steel	C	Cr	Ni	Mo	σ_y (MPa)	σ_u (MPa)	A (%)	HV
F-138	0.025	17.5	14.0	2.8	190	490	45	170
AISI 316L	0.030	17.0	12.0	2.2	240	450	40	–

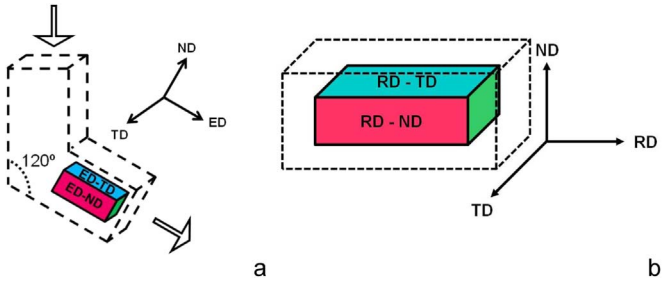

Fig. 1. Schematic representation of the shape of the samples cut for XRD and EBSD analysis and the corresponding reference directions from a) ECAE and b) rolled samples.

100 μm × 100 μm resolution. The instrumental broadening was calibrated using a NIST LaB_6 standard.

The same samples were used for EBSD analysis, where the two surfaces presented in Fig. 1 were analyzed. They were ground and then polished using 9, 6, 3 and 1 μm diamond paste and 0.05 μm colloidal silica. The EBSD measurements were performed in an FEI Quanta 200 FEG-SEM, with EDAX OIM hardware plus software. The lowest misorientation to define a grain border was set to 1.0°, slightly larger than the 0.5° accepted as the minimum angular resolution for EBSD.

Small disks were cut from E1X, E2X and R70 samples for TEM analysis. They were thinned with a 10% perchloric acid in ethanol solution at 10 °C and 30 V and analyzed in a Philips CM120 microscope. Vickers Hardness (HV10) was also measured in order to determine the recrystallization temperature.

4. Results

The mechanical properties and Vickers hardness measurements obtained for the As Received and deformed samples are presented in Table 2. It can be seen from this table and from Fig. 2 that the hardness increases with ECAE passes and is even larger for the cold rolled sample, even though the equivalent von Mises deformation is quite similar. Hardness did not change appreciably after annealing at 600 °C and 700 °C, but presented a sharp decrease at 800 °C, which might be related to the formation of recrystallized grains.

TEM images obtained for the extruded and cold rolled samples are presented in Fig. 3. Both ECAE passes show the presence of both twins and dislocation cells, while for the cold rolled sample a set of many thin twin-like structures are observed, and more dislocation arrays. This situation implies that ECAE seems to be more effective than cold rolling for twinning, while cold rolling would lead to a higher dislocation density. Besides, these nano-twins observed after cold rolling might not be interpreted correctly by the diffraction techniques that will be used ahead. A stacking fault density of approximately 4 stacking faults per micron can be estimated for the sample deformed by ECAE, that rises to 40 μm^{-1} after 2 pressings, similar to 30 μm^{-1} found for the cold rolled sample.

4.1. X-ray diffraction

Williamson-Hall and CMWP methods were applied in the samples deformed by ECAE and cold rolled and annealed at 600 °C and 700 °C. Measurements were performed also for the samples annealed at 800 °C

Table 2
Hardness and mechanical properties of F138 steel deformed by ECAP and cold rolling.

Sample	σ_y (MPa)	σ_u (MPa)	ε_t (%)	ε_u (%)	HV	$\varepsilon_{von\ Mises}$
Initial	374	640	60	23	130	0
E1X	889	907	36	2.8	321	0.67
E2X	1055	1108	28	2.8	339	1.34
R70	1100	1135	32	3.5	374	1.3

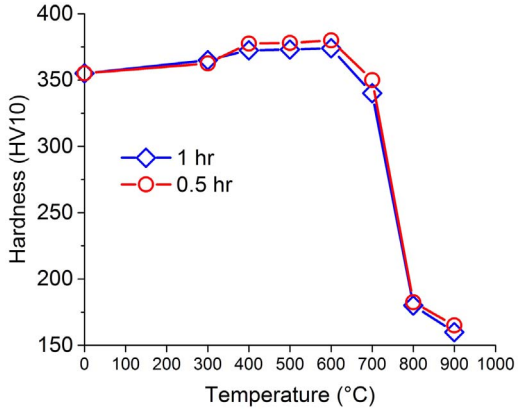

Fig. 2. Vickers hardness measured on the cold rolled samples after annealing at different temperatures.

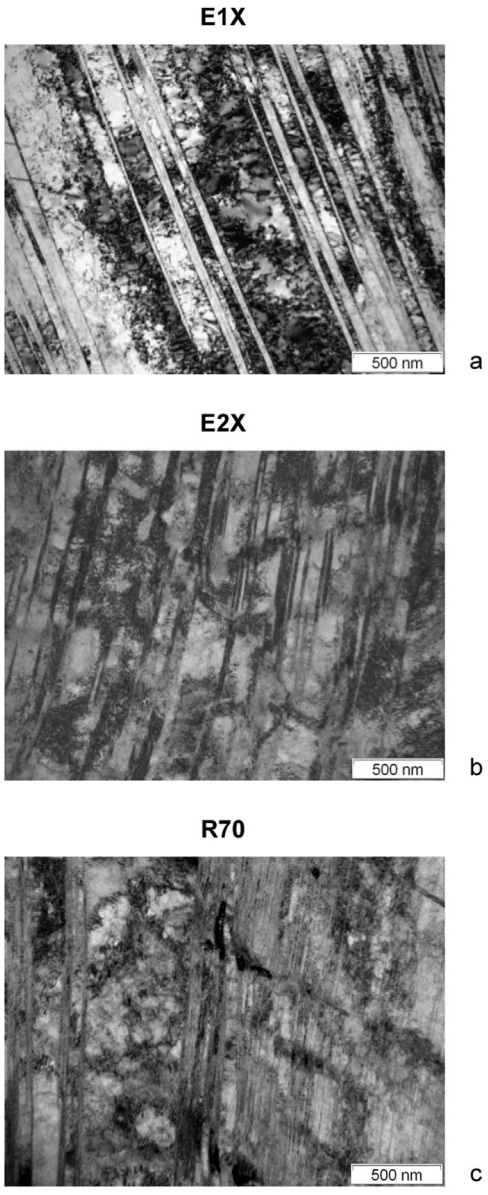

Fig. 3. TEM images obtained for samples deformed by ECAE ((a) 1 and (b) 2 pressings) and (c) cold rolling (40000X).

and 900 °C but the large grain microstructure did not allow to obtain full Debye-Scherrer rings, instead only spotted patterns that did not contain enough data when partitioned; therefore, they were excluded from the XRD analysis, but they will be considered again in the next section.

Average domain size and stacking fault density obtained using both methods along the three perpendicular directions mentioned in Fig. 1 are presented in Fig. 4. Regarding domain size, it can be seen in Fig. 4**(a)** and **(b)** that the behavior of the values is quite similar using both methods. The sample deformed in 1 ECAE press shows similar domain size along TD and ND and smaller size along ED; this seems to be consequence of the deformation geometry, where the maximum strain occurs in plains inclined about 60° to the extrusion direction, which causes grain fragmentation in ED. After performing the second pass with a 90° rotation, the direction of maximum strain changes and the domains become more equiaxed, which is observed in the present results. A different situation is observed in the cold rolled samples, where after deformation the domains are slightly larger along RD and smaller along ND, in agreement with the typical "plate-like" microstructure observed in rolled materials. With increasing annealing temperature, the domain size increases slightly along ND and TD but becomes larger than 100 nm along RD, which might indicate that these samples are at the onset of recrystallization. The realization that the recrystallization is not complete originates in the fact that the values are not the same for all directions, indicating that domains are not equiaxed. The fact that the variation is more obvious in CMWP results than in W-H might be a consequence of the different processes employed by both methods to separate the instrumental contribution to broadening. Small peak broadening can be caused by small dislocation density, large grains or small instrumental contribution, and if the latter is not accounted for correctly, the causes of broadening can be mixed up.

The results obtained for stacking fault density present more dispersion with respect to sample direction in W-H than in CMWP, and the main observation is that 2 cycles of ECAE pressing create more stacking faults than cold rolling. This result indicates that, even though the equivalent von Mises deformation is similar for these samples, the geometrical characteristics of the processing cause different twin boundary development. The values estimated using TEM were not very different between both samples, although two remarks can be made: the value for the rolled sample is smaller than for 2 ECAE pressings, and both are of the same order as those obtained in TEM.

Dislocation densities estimated by both methods are presented in Fig. 5. CMWP allows the determination of both, dislocation density and dislocation arrangement parameter M*, while W-H only provides a strain-related factor than includes both values but does not disclose them individually. Therefore, the results in Fig. 5 are calculated from this factor in W-H by tuning the M* values obtained in CMWP (Fig. 5**(c)**) as was explained in a previous paper [13]. Increasing number of ECAE pressings resulted in higher dislocation density, and according to CMWP cold rolling caused similar or less dislocation storage than 2 ECAE cycles, that then decreased with annealing at 600 °C and 700 °C (but not changing substantially with temperature). The heterogeneity in the values obtained for different directions for the sample pressed 2 times will be discussed ahead. Regarding M*, the values obtained for all the samples were smaller than 1, indicating a high amount of compact arrays of dislocations.

4.2. Electron Backscatter Diffraction

EBSD has become the technique of choice for studying the defects caused on the microstructure by severe deformation [27–29]; while maps show the complexity of the microstructure, the charts allow to quantify the amount and degree of misorientation of boundaries and to characterize strain localization.

One of the experimental settings of great importance in the analysis

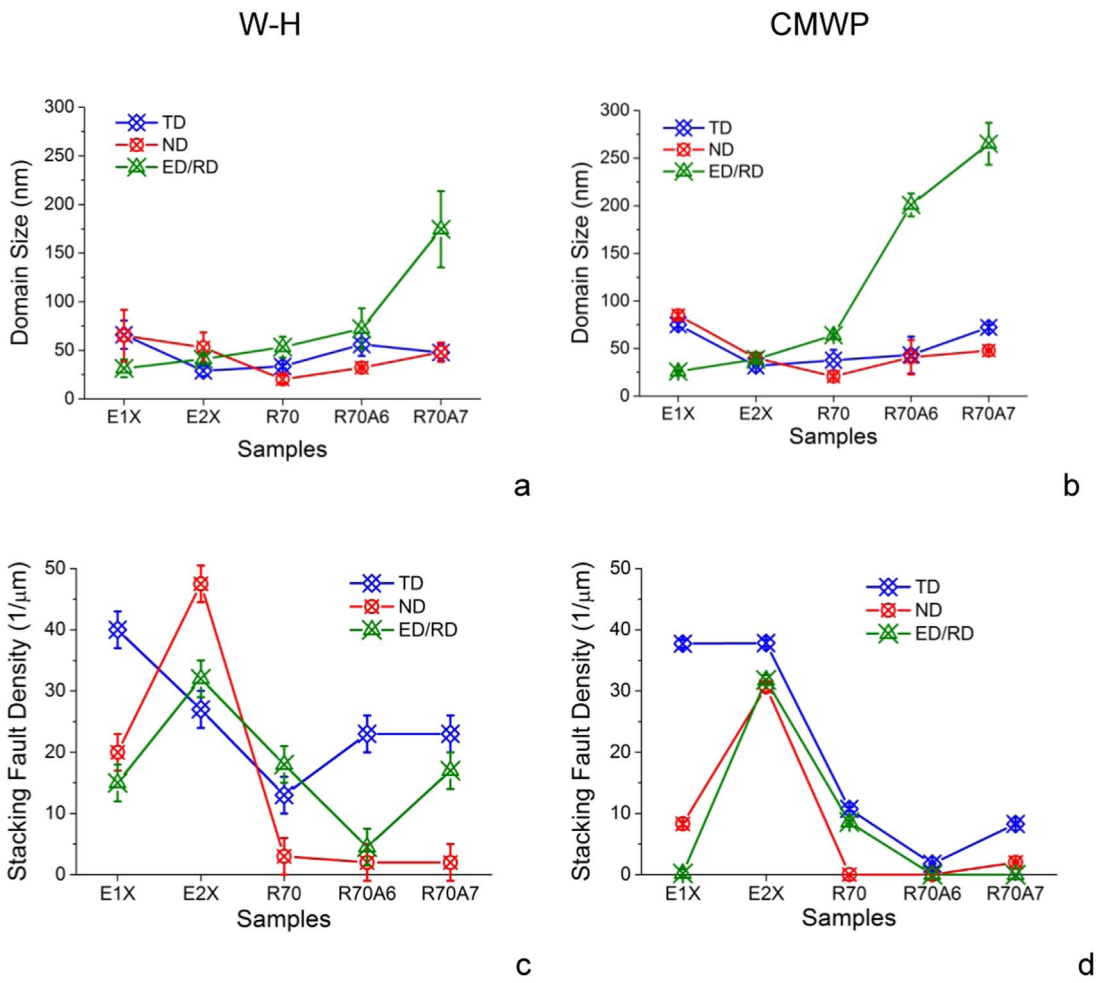

Fig. 4. Average domain size ((a) WH and (b) CMWP) and stacking fault density ((c) W-H and (d) CMWP) obtained for all the samples.

is the election of the step size to be used. It is recommended that, in order to obtain a 10% error in the measurement of a microstructural feature, the step size to be used should be approximately one tenth of the size of the feature to be analyzed [30]. For the current samples the diffraction domains detected by X-ray diffraction were smaller than 100 nm, and 10 nm in step size, taking into account the advised rule, would be lower than the resolution limit of the equipment. The step size used in the current analysis was 70 nm; some of the nanometric characteristics of the sample could be missed, but data, complementary to XRD results, can still be obtained with the purpose of analyzing scale influence on microstructure behavior.

Inverse Pole Figure maps (IPF) are presented in Figs. 6 and 7 for the ECAE pressed samples, the cold rolled and annealed at 600° and 700 °C and annealed at 800° and 900 °C, respectively. These last two recrystallized samples were only analyzed in TD-RD surface for comparison of the microstructure with the deformed states.

The different mechanical processing, ECAE and cold rolling, give rise to differences in microstructure that can be seen in those figures,

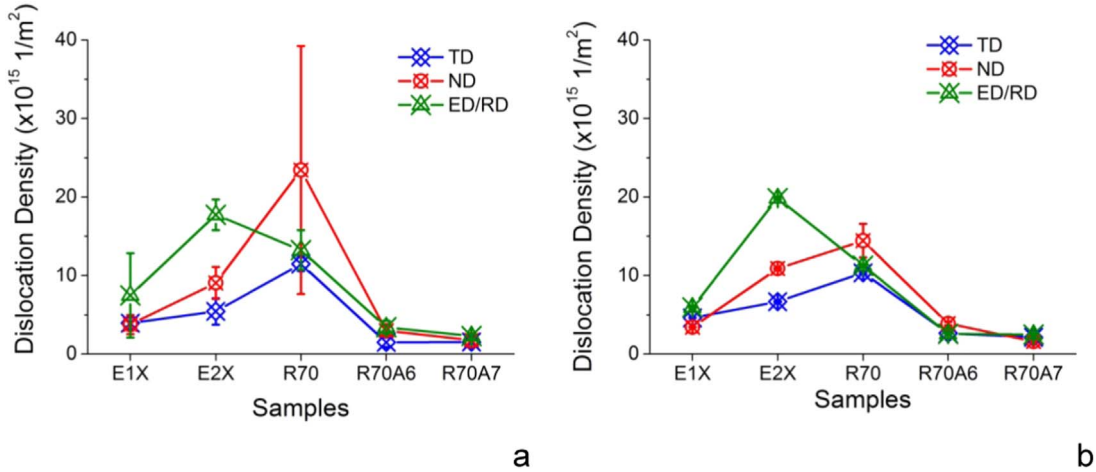

Fig. 5. Dislocation density obtained for all the samples ((a) calculated from W-H and (b) by CMWP).

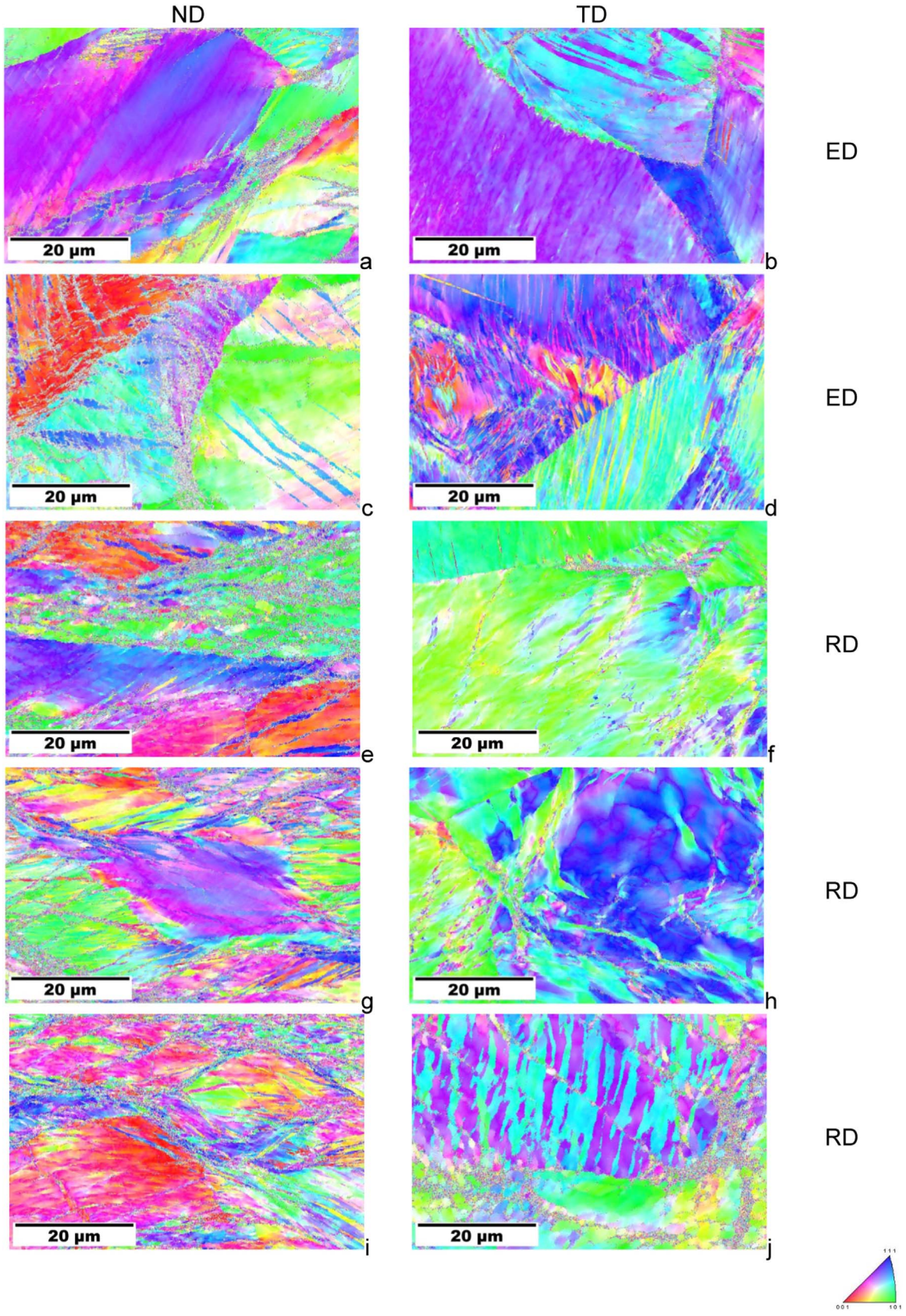

Fig. 6. IPF maps on the ND-ED (1st col.) and TD-ED (2nd col.) planes for a)-b) E1X and c)-d) E2X, and for the ND-RD (1st col.) and TD-RD (2nd col.) planes for e)-f) R70, g)-h) R70A6 and i)-j) R70A7.

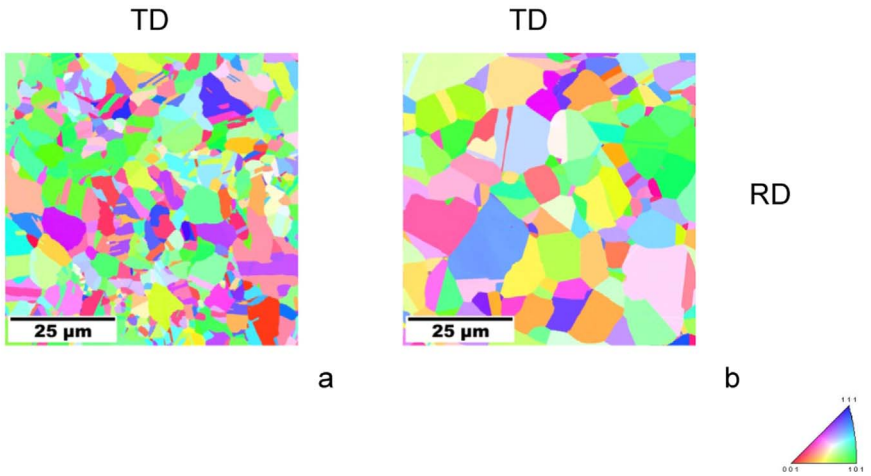

Fig. 7. IPF maps on the ND-RD planes for a) R70A8 and b) R70A9 samples.

mainly in ED-ND and RD-TD maps. A single pass in ECAE deformation determines a microstructure of diagonal misorientation boundaries where some boundaries present an inclination of ~ 60°, which is characteristic of the processing considering a 120° angle between the channels intersecting in the die. If the second pressing would have occurred without rotation of the sample, a similar structure would be visible in Fig. 6**(c)** but also with 30° inclined bands, but since the deformation route followed in these study consisted in rotating the sample 90° between consecutive passes, this band-oriented structure is no longer observed; instead, thicker bands of poorly-indexed points are observed, indicating a higher accumulation of strain inside these bands. However, some bands inclined in 60° are observed in the top surface in Fig. 6**(d)** (TD-ED), which are remnant of the first pressing and did not suffer from crossed twinning during second pass.

Cold rolling microstructure in RD-ND planes is elongated along RD as expected from the deformation geometry, and remains similar in aspect ratio after annealing at 600 °C and 700 °C, but some "cleaner" or less misoriented areas appear with thicker boundaries between them. This could indicate that early stages of recrystallization or recovery are taking place.

Considering all the information obtained from the observation of the microstructure, the focus moves on to the analysis of the quantitative data. The first step into this analysis is the definition of a criterion that must be met by pixels in order to be considered belonging to the same grain. For these samples, the criterion was that a grain must be composed of a minimum of 3 pixels and a minimum boundary misorientation of 3°. Grain size (calculated using the "Intercept Lengths" tool available in OIM) is plotted in Fig. 8. These values are larger than XRD domain sizes by more than 1 order of magnitude, which is probably a consequence of the step size used, but it is interesting to note that the correlation between the values at different deformation stages and annealing temperatures remains quite similar. This result validates the use of a non ideal step size, which in this case shows a correlation between different scales.

The analysis turns now to the character of the misorientation boundaries developed in the samples (Fig. 9). In order to analyze separately gran boundaries and boundaries inside the defined grains, the criteria used to separate High Angle and Low Angle boundaries was set to 3°. CSL (Coincidence Site Lattice) boundaries were considered for this FCC steel as $\Sigma 3^n$ boundaries [30]. Since three scans were performed on each surface of the samples and not all the scans were of the same area, the number of boundaries of each character were calculated and then normalized on the number of pixels of the scans involved. It can be seen that in E2X and R70 in ED-ND and RD-ND planes the amount of HAGBs is larger than that of LAGBs, which might indicate a smaller dislocation accumulation inside the grains in the scans in this surface. A similar situation happens in both planes for R70A6 sample, which contributes to the hypothesis that recrystallization is beginning; however, this situation is not observed in R70A7 for the sum of scans, but was indeed observed in one of the three scans, indicating that this phenomenon is only of local character at this point. Annealing at 800 °C and 900 °C caused a decrease in grain boundary density. Focusing in particular in E2X and R70 results, it can be seen that the latter presents a larger amount of boundaries than the former, mainly in RD-TD planes, and focusing in boundaries smaller than 3° it can be stated that dislocation density inside grains for the cold rolled sample could be larger than for 2 ECAE pressings. However, a consideration must be made in this matter: this larger amount of LAGBs indicates that more

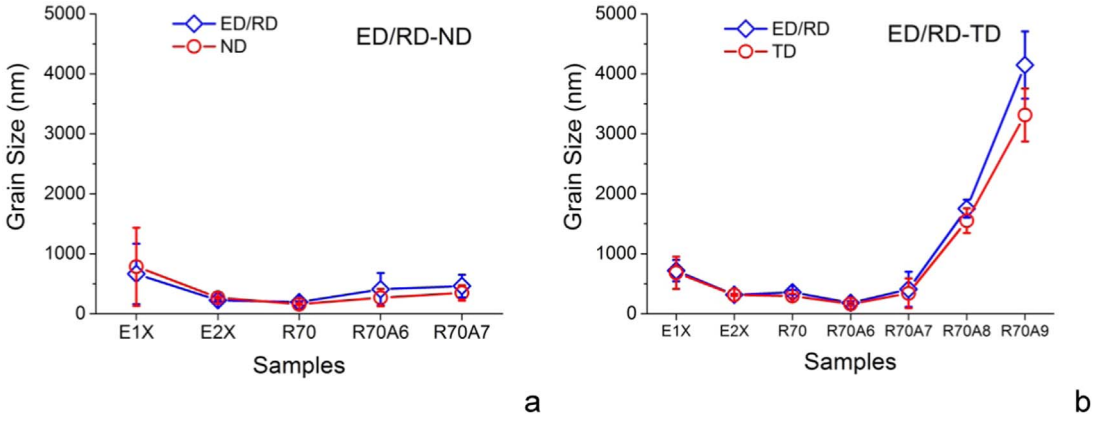

Fig. 8. Grain size calculated by the Intercept Lengths method.

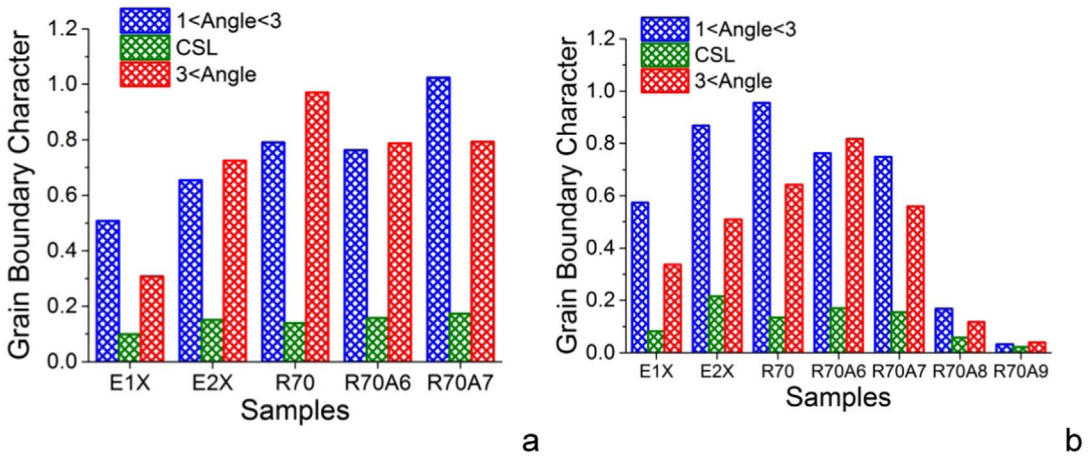

Fig. 9. Grain boundary character distributions per unit area obtained for both analyzed surfaces in each sample.

boundaries are found, which could be indicating a larger amount of dislocations in these boundaries, but this does not give any information regarding dislocations that are not forming arrays, which are "invisible" for EBSD.

Having analyzed grain size and boundaries, the analysis focuses now in local accumulation of dislocations inside grains. This analysis was performed both in a quantitative and qualitative approach. First, Geometrically Necessary Dislocation density was determined in order to be compared quantitatively with XRD results. Fig. 10 presents the values obtained in each surface. A first evaluation of the data supplies that all values are on the order of 10^{14} m^{-2}, which is about 2 orders of magnitude smaller than the dislocation density obtained in W-H and CMWP; the reason for this difference is that EBSD only allows to detect dislocations that are forming arrays and causing a misorientation in the crystal structure, which implies that looser arrays are not being detected by this technique, but XRD is sensitive to the small effect they have in the strain field. The values in Fig. 10 are large when the LAGB values are large, which is consistent with the exclusion of misorientations > 3° in favor of considering them as grain boundaries. These data show an increase with ECAE pressings, and similar values but for opposite surfaces in the cold rolled sample; after annealing at 600° and 700° the values decrease slightly, but then diminish sharply after 800 °C. This also supports the observations made before regarding the level or recrystallization present in the samples, because this process is related to "cleaner" or less misoriented grains, hence with fewer amounts of dislocations.

In order to get an insight on the local character of the misorientation distribution inside grains, Grain Orientation Spread (GOS) was calculated (Fig. 11). For the samples deformed in ECAE, it can be seen that

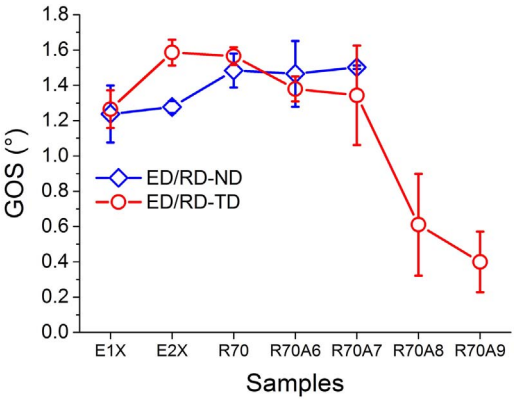

Fig. 11. Grain orientation spread.

higher deformation lead to an increase in GOS; this indicates that the spread of misorientations across the grains also increased. There is a proportional correspondence between GOS and GND increments and decrements. Similar GOS values were obtained for the cold rolled and annealed at 600° and 700 °C samples (with a slight decrease but increasing dispersion) and then they decrease for annealing at 800° to values smaller than 1°.

Finally, stacking fault density was calculated for these samples (Fig. 12). As was presented and mentioned in previous papers [13,31], these values were about 2 orders of magnitude smaller that the results obtained by XRD and TEM, which indicates that the nano-twins present in the samples cannot be detected by the resolution of the technique.

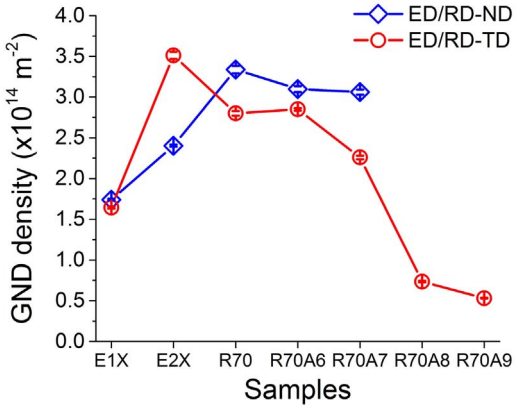

Fig. 10. Geometrically necessary dislocation density obtained in OIM for ECAE and cold rolled and annealed samples.

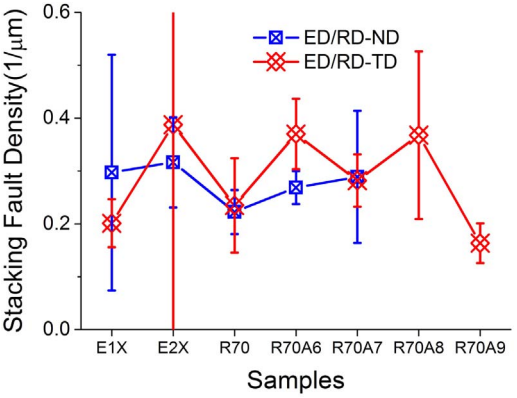

Fig. 12. Stacking fault densities determined by EBSD.

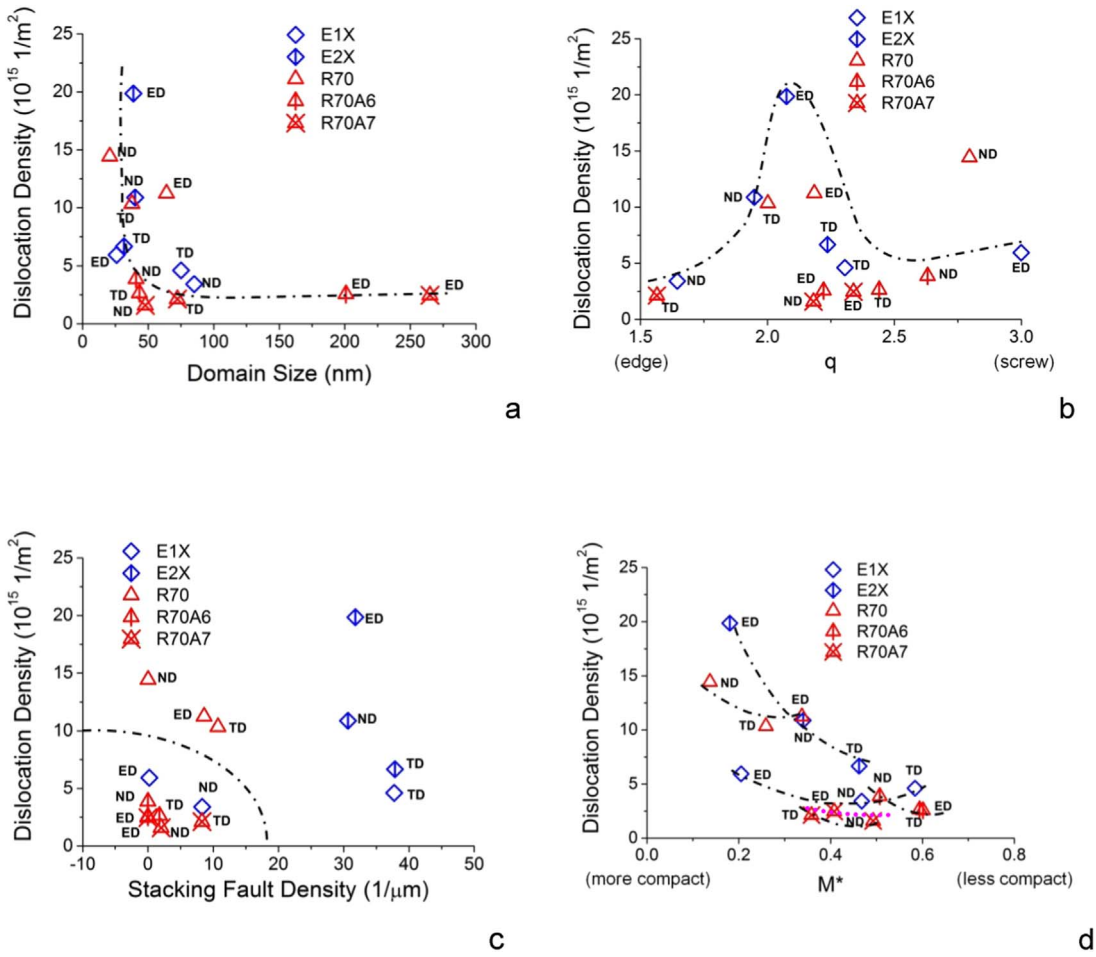

Fig. 13. Plots representing the dislocation density dependence on other microstructural parameters: a) domain size, b) stacking fault density, c) *q* and d) *M* parameters (dot and dash lines are only eye guides).

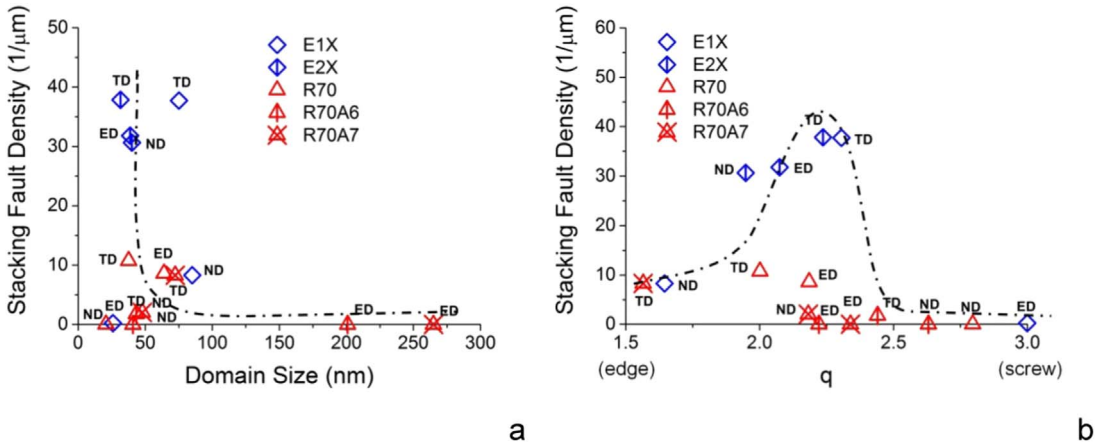

Fig. 14. Plots showing the variation of stacking fault density with respect to a) the domain size and b) the *q* parameter (dot and dash lines are only eye guides).

5. Discussion

X-ray diffraction, as one of the most powerful diffraction techniques to study the microstructure of materials, allowed, as a first step, to obtain quantitative information regarding the changes undergone by the microstructure during a particular thermomechanical process. However, on a deeper analysis, different relationships between the microstructural parameters can be obtained, granting information on the correlation between these parameters. The graphs in Figs. 13 and 14 present the correlation between dislocation and stacking fault density with domain size, dislocation character **q** and arrangement parameter **M***. The same graphs were plotted in Figs. 14 and 15 in a previous paper for samples deformed by ECAE up to 4 times at room temperature and 300 °C, and the correlation between the values is quite similar [13]. Larger dislocation densities were found in samples and directions with small domain size and vice versa Fig. 13**(a)**, and a similar behavior was observed in Fig. 14**(a)** for stacking faults. Regarding dislocation character (q), both dislocation and stacking fault densities seem to present their largest values for similar proportion of edge and screw dislocations (Figs. 13**(b)** and 14**(b)**). Fig. 13**(c)** presents the relationship

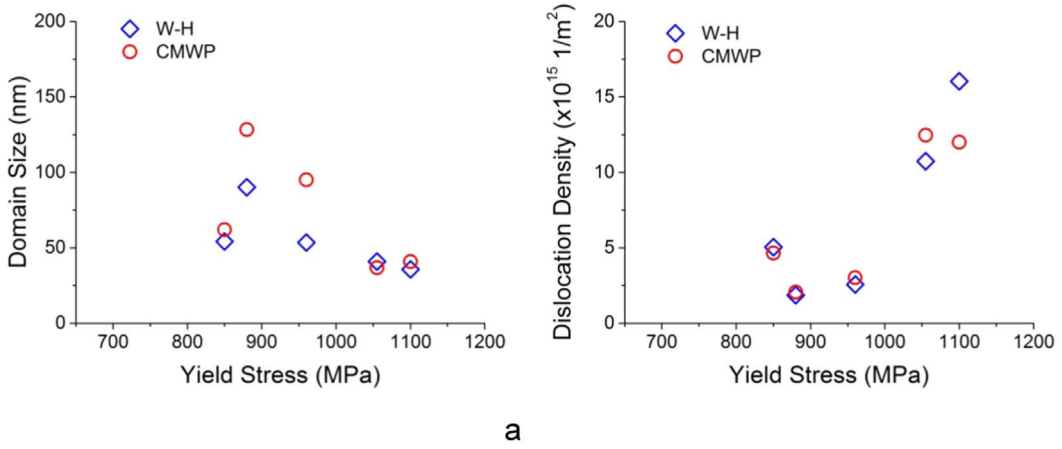

Fig. 15. Variation of a) domain sizes and b) dislocation density with respect to the Yield Stress. The behavior of the data is consistent with Eq. (3), corresponding to Kocks-Mecking model.

between dislocation and stacking fault density, and two populations seem to appear where both values are high or low. High values are found mainly for E2X and R70 samples, which present similar and high von Mises deformation. This situation was observed in the mentioned paper for the samples deformed by ECAE at room temperature. It must be remarked that, in the present case, E2X sample presented higher stacking fault density than R70 and similar dislocation densities with a higher dispersion. The finer microstructure in ECAE samples seems to be consequence of the refining effect provided by the higher activity of twining. Finally, Fig. 13**(d)** presents the relationship between dislocation density and their arrangement parameter M*. As in the mentioned paper, lower dislocation densities corresponded to larger values of M*, hence to less compact arrays. The curve with fastest descent corresponds to E2X sample, which corresponds to a high dispersion between the values determined along each direction.

It must be emphasized that domain size is expected to depend mostly on the direction of analysis, because the grain shape depends highly on the external loading conditions imposed to the sample. It is expected that both grain size and shape are not dependent on the crystal orientation since they are not physical material properties. Dislocation and stacking fault densities, however, are intrinsic physical properties that depend on the micromechanical mechanisms activated during the particular deformation process employed. However, because twin density is obtained fundamentally as a consequence of its influence on grain size, although with a different (*hkl*) dependence, the detected twin boundaries are numerically different when observed in the same grain in different directions. So, regarding its detectability, they behave more as grain boundaries than as dislocation arrays.

Obtaining different dislocation densities when analyzing different directions might appear contradictory, considering that this value corresponds to the length of dislocations per unit volume, but there are several factors influencing the measurement:

- Since the samples are analyzed in transmission, different crystals are participating in diffraction when the sample rotates, which can lead to different dislocation densities.
- Average contrast factors were used for these samples. This might not be the optimum choice for these samples, even though the intensity in texture measurements were not large.

In spite of all this situations, average domain sizes and dislocation densities should behave according to the Kocks-Mecking equation for grain refinement at large strains [32]:

$$d\rho/d\sigma = k_0/\mathrm{bd} - k_2\rho \quad (3)$$

where d is cell size (measured as the mean free path for dislocations), ρ the dislocation density, σ the yield stress, b the Burgers vector and k_0 and k_2 are constants. This model considers that, during a deformation process, dislocations contribute to grain refinement by forming compact arrays. In a previous paper, where samples deformed by ECAE at room temperature and at 300 °C were analyzed, the values obtained for the samples agreed with this model [13], and as can be seen in Fig. 15 in the present paper there is also a similar behavior for the present samples: higher Yield stresses are related to smaller domain sizes and larger dislocation densities.

EBSD provided different kind of information related to the microstructure that can be combined with the data obtained by XRD. A first comment must be performed regarding grain size, where although the step size used did not allow an accurate determination of the size of the structures, a good correlation was found for these samples at different scales. Comparing XRD calculated dislocation density with GND density and GOS determined by EBSD a very good correlation is found, indicating that step size does not seem to be an important factor for local strain analysis. Nonetheless, it must be stated that the chosen step size was at least of the same order of the size of the features to be quantified; if the step size would have been larger than 100 nm this would have not been the case, and the scale correspondence could be lost.

A final discussion must be devoted to the comparison in depth of the microstructures developed in the samples that present similar von Mises deformation (E2X and R70). At a first glance, it seems that both XRD and EBSD show that domain sizes are not different between these samples (between 25 and 50 nm approximately in XRD), but considering the results obtained in XRD for the three different directions (mainly in CMWP analysis) it seems that 2 ECAE pressings in route B_C are more effective for grain refinement than cold rolling up to the same level of deformation, and even accomplishing equiaxed domains. Stacking fault density was also found to be larger for E2X, which could contribute to both domain refinement and equiaxiality. Regarding dislocation density, CMWP results show a larger spread for E2X than for R70 but the averages are similar. This added to GBCD charts (which show similar behavior for both samples in each surface) and GND and GOS results, shows that there is a difference in which kind of dislocations and characteristic arrays develop in each sample, but not a substantial difference in the refinement of the microstructure can be observed, except for the inclusion of profuse twining in ECAE samples. In fact, sometimes mechanical properties present advantageous values for R70 sample in comparison with 2X sample.

6. Conclusions

X-ray and Electron Backscatter Diffraction have been used for the microstructural analysis of samples of F138 stainless steel subject to different deformation processes.

A good correlation was found between the different results that both techniques allow to obtain, which translated also in a good correspondence in the analysis at different scales. Domain sizes decreased with 2 ECAE pressings in route B_C with a development of equiaxed subgrains and an increase in dislocation and stacking fault density. Cold rolling, on the other hand, caused domains of similar order than 2 ECAE pressings but with larger dispersion showing larger value along RD, which then increased in value and in difference with the other directions after annealing at 600 and 700 °C. Dislocation density increased with ECAE pressings, and similar values in average were found for the cold rolled sample, which then decreased with annealing temperature.

A good correlation was found between these results and EBSD, where grain size decreased with ECAE and cold rolling and GND and GOS increased, and the opposite situation was observed after annealing at higher temperatures.

Samples with similar von Mises equivalent deformation showed differences in the microstructure, indicating that 2 ECAE passes are slightly more effective than cold rolling for grain refinement and production of equiaxed domains, mainly because of a larger activation of twins, but with no substantial increase in dislocation density and/or mechanical properties.

It is known that in monotonic deformation the twin activity diminishes drastically after a few percent deformation [33]. The continuous strain path because of continuous macroscopic spin during ECAE and the extra external spin after each ECAE pass provides further opportunity for secondary twinning to become active more homogeneously inside each grain and evenly distributed for all grains, sources for extra refinement of microstructure.

Finally, it can be concluded that a high correlation can be obtained for both techniques, despite their different spatial and angular resolution and somehow different quality of defects detected by them. A scale invariance can be inferred between the limits of detection, that is, the defects tend to accumulate showing similar behaviors on the studied categories. Moreover, whenever they do not clearly match, the results can be rationalized attending some particularities of the technics.

Acknowledgments

The authors would like to thank Prof. Tamás Ungár, Prof. Adam Révész and Dr. Levente Balogh for their assistance in the use and applications of CMWP software. Authors are grateful to Lic. Vanina Tartalini and Bioeng. Pablo Risso for their help in sample preparation and camera optimization for EBSD.

This research has been funded by the FAPESP — Brazil (Grant number 2011/02009-0); ANPCyT — Argentina, Grant PID-BID 1341 and the International Collaboration CONICET, Argentina–DFG, Germany (Resolution No: 0183/13).

References

[1] F. Liu, Y. Zhang, J.T. Wang, Microstructure evolution of pure nickel up to a high strain level during equal-channel angular pressing, Mater. Sci. Forum 667–9 (2011) 319–324.

[2] Y. Zhang, N.R. Tao, K. Lu, Effects of stacking fault energy, strain rate and temperature on microstructure and strength of nanostructured Cu–Al alloys subjected to plastic deformation, Acta Mater. 59 (2011) 6048–6058.

[3] C. Barrett, T.B. Massalski, Structure of Metals, 3rd revised ed., Pergamon Press, Oxford, 1980, p. 395.

[4] G.K. Williamson, W.H. Hall, X-ray line broadening from filed aluminum and wolfram, Acta Metall. 1 (1953) 22–31, http://dx.doi.org/10.1016/0001-6160(53)90006-6.

[5] T. Ungár, J. Gubicza, G. Ribárik, A. Borbély, Crystallite size distribution and dislocation structure determined by diffraction profile analysis: principles and practical application to cubic and hexagonal crystals, J. Appl. Cryst. 34 (2001) 298–310, http://dx.doi.org/10.1107/S0021889801003715.

[6] T. Ungár, J. Gubicza, P. Hánák, I. Alexandrov, Densities and character of dislocations and size-distribution of subgrains in deformed metals by X-ray diffraction profile analysis, Mater. Sci. Eng. A 319-321 (2001) 274–278, http://dx.doi.org/10.1016/S0921-5093(01)01025-5.

[7] B.E. Warren, X-ray studies of deformed metals, Prog. Met. Phys. 8 (1959) 147–202, http://dx.doi.org/10.1016/0502-8205(59)90015-2.

[8] G. Ribárik, Modeling of Diffraction Patterns Based on Microstructural Properties, Ph.D. Thesis, 2008. ⟨http://csendes.elte.hu/cmwp/doc/Ribarik-PhD-Thesis.pdf⟩.

[9] A.J. Schwartz, M. Kumar, B.L. Adams, Electron Backscatter Diffraction in Materials Science, 2nd ed., Klawer Academic-Plenum Publishers, New York, 2000.

[10] S. Curtze, V.T. Kuokkala, A. Oikari, J. Talonen, H. Hänninen, Thermodynamic modeling of the stacking fault energy of austenitic steels, Acta Mater. 59 (2011) 1068–1076.

[11] A. Das, Revisiting stacking fault energy of steels, Metall. Mater. Trans. A 47 (2016) 748–768.

[12] S. Scheriau, Z. Zhang, S. Kleber, R. Pippan, Deformation mechanisms of a modified 316L austenitic steel subjected to high pressure torsion, Mater. Sci. Eng. A 528 (2011) 2776–2786, http://dx.doi.org/10.1016/j.msea.2010.12.023.

[13] N.S. De Vincentis, A. Kliauga, M. Ferrante, M. Avalos, H.-G. Brokmeier, R.E. Bolmaro, Evaluation of microstructure anisotropy on room and medium temperature ECAP deformed F138 steel, Mater. Charact. 107 (2015) 98–111, http://dx.doi.org/10.1016/j.matchar.2015.06.035.

[14] N.S. De Vincentis, M.C. Avalos, E.A. Benatti, A. Kliauga, H.-G. Brokmeier, R.E. Bolmaro, XRD and EBSD analysis of anisotropic microstructure development in cold rolled F138 stainless steel, Mater. Charact. 123 (2017) 137–152, http://dx.doi.org/10.1016/j.matchar.2016.11.018.

[15] P. Scherrer, Bestimmung der Größe und der inneren Struktur von Kolloidteilchen mittels Röntgenstrahlen, Göttinger Nachrichten Gesell 2 (1918) 98–100 ⟨http://gdz.sub.uni-goettingen.de/dms/load/img/?PPN=GDZPPN002505045&IDDOC=63709⟩.

[16] G. Caglioti, A. Paoletti, F. Ricci, Choice of collimators for a crystal spectrometer for neutron diffraction, Nucl. Instrum. Methods 3 (1958) 223–228.

[17] T. Ungár, I. Dragomir, A. Révész, A. Borbély, The contrast factor of dislocations in cubic crystals: the dislocation model of strain anisotropy in practice, J. Appl. Cryst. 32 (1999) 992–1002, http://dx.doi.org/10.1107/S0021889899009334.

[18] I.C. Dragomir, T. Ungár, Contrast factors of dislocations in the hexagonal crystal system, J. Appl. Cryst. 35 (2002) 556–564, http://dx.doi.org/10.1107/S0021889802009536.

[19] D.A. Hughes, N. Hansen, D.J. Bammann, Geometrically necessary boundaries, incidental dislocation boundaries and geometrically necessary dislocations, Scr. Mater. 48 (2) (2003) 147–153, http://dx.doi.org/10.1016/S1359-6462(02)00358-5.

[20] G. Ribárik, J. Gubicza, T. Ungár, Correlation between strength and microstructure of ball-milled Al–Mg alloys determined by X-ray diffraction, Mater. Sci. Eng. A 387–389 (2004) 343–347, http://dx.doi.org/10.1016/j.msea.2004.01.089.

[21] G. Ribárik, T. Ungár, Characterization of the microstructure in random and textured polycrystals and single crystals by diffraction line profile analysis, Mater. Sci. Eng. A 528 (2010) 112–121, http://dx.doi.org/10.1016/j.msea.2010.08.059.

[22] P. Ducheyne, G.W. Hastings, CRC Series on Structure–Property Relationships of Biomaterials, CRC Press, Boca Raton, FL, 1984.

[23] M. Semlitsch, P. Ducheyne, G.W. Hastings (Eds.), Metals and Ceramics Biomaterials, CRC Press, Boca Raton, FL, 1984, pp. 1–21.

[24] L.S. Mannan, C.S. Chetal, B. Raj, B.S. Bhoje, Selection of materials for prototype fast breeder reactor, Trans. Indian Inst. Met. 56 (2) (2003) 155–178.

[25] J.P. Strizak, H. Tian, P.K. Liaw, L.K. Mansur, Fatigue properties of type 316LN stainless steel in air and mercury, J. Nucl. Mater. 343 (1–3) (2005) 134–144, http://dx.doi.org/10.1016/j.jnucmat.2005.03.019.

[26] Y. Iwahashi, J. Wang, Z. Horita, M. Nemoto, T.G. Langdon, Principle of equal-channel angular pressing for the processing of ultra-fine grained materials, Scr. Mater. 35 (1996) 143–146, http://dx.doi.org/10.1016/1359-6462(96)00107-8.

[27] Y.J. Chen YJ, J. Hjelen, H.J. Roven, Application of EBSD technique to ultrafine grained and nanostructured materials processed by severe plastic deformation: sample preparation, parameters optimization and analysis, Trans. Nonferrous Met. Soc. China 22 (2012) 1801–1809, http://dx.doi.org/10.1016/S1003-6326(11)61390-3.

[28] E. Bonnot, A.L. Helbert, F. Brisset, T. Baudin, Microstructure and texture evolution during the ultra grain refinement of the Armco iron deformed by accumulative roll bonding (ARB), Mater. Sci. Eng. A 561 (2013) 60–66, http://dx.doi.org/10.1016/j.msea.2012.11.017.

[29] F. Cruz-Gandarilla, A.M. Salcedo-Garrido, R.E. Bolmaro, T. Baudin, N.S. De Vincentis, M. Avalos, J.G. Cabañas-Moreno, H. Mendoza-Leon, Microstructural evolution and mechanical properties on an ARB processed IF steel studied by X-ray diffraction and EBSD, Mater. Charact. 118 (2016) 332–339, http://dx.doi.org/10.1016/j.matchar.2016.05.025.

[30] V. Randle, Electron backscatter diffraction: Strategies for reliable data acquisition and processing, Mater. Charact. 60 (2009) 913–922, http://dx.doi.org/10.1016/j.matchar.2009.05.011.

[31] N.S. DeVincentis, Microstructural investigation of materials by a combination of Electron Backscatter Diffraction (EBSD and X-ray diffraction (XRD) techniques, Ph. D. Thesis, 2015.

[32] U.F. Kocks, H. Mecking, Physics and phenomenology of strain hardening: the FCC case, Prog. Mater. Sci. 48 (3) (2003) 171–273, http://dx.doi.org/10.1016/S0079-6425(02)00003-8.

[33] E. El-Danaf, S.R. Kaldindi, R.D. Doherty, Influence of grain size and stacking-fault energy on deformation twinning in fcc metals, Met. Mater. Trans. A 30 (1999) 1223–1233, http://dx.doi.org/10.1007/s11661-999-0272-9.